The impact of solid solution composition on kinetics and mechanism of [2 + 2] photodimerization of cinnamic acid derivatives

Lorenzo Pandolfi, Andrea Giunchi, Tommaso Salzillo,* Aldo Brillante, Raffaele G. Della Valle, Elisabetta Venuti,* Fabrizia Grepioni, and Simone D'Agostino*

The impact of solid solution composition on kinetics and mechanism of [2+2] photodimerizations of cinnamic acid derivatives

CrystEngComm, 2021, 23, 1352–1359

The impact of solid-solution composition on kinetics and mechanism of [2+2] photodimerizations of cinnamic acid derivatives

Lorenzo Pandolfi,[†a] Andrea Giunchi,[†a] Tommaso Salzillo,*[ab] Aldo Brillante,[a] Raffaele G. Della Valle,[a] Elisabetta Venuti,*[a] Fabrizia Grepioni,[c] and Simone D'Agostino*[c]

[a] *Dipartimento di Chimica Industriale "Toso Montanari", Università di Bologna, viale del Risorgimento, 4, 40136, Bologna.*

[b] *Department of Materials and interfaces, Weizmann Institute of Science, Herzl street 234, 76100 Rehovot, Israel.*

[c] *Dipartimento di Chimica "Giacomo Ciamician", Università di Bologna, Via Francesco Selmi, 2, 40126, Bologna, Italy.*

[†] These authors contributed equally to this work.

Electronic Supplementary Information (ESI) available: single crystal data and refinement details, powder X-ray diffraction patterns, FTIR and Raman spectra, representation of the PCA method, and kinetic scheme. See DOI: 10.1039/x0xx00000x

Abstract

We propose the use of *solid-solutions* for the modulation of the kinetic in [2+2] photocycloaddition. Solid-solutions with general formula [**1**H]Br_xCl_{1-x} (**1** = 4-amino-cinnamic acid; 0 < x < 1) were prepared via mechanochemical methods, structurally characterized, and found to undergo a single-crystal-to-single-crystal [2+2] photodimerization. The effect of the solid-solutions composition on the kinetics was successfully investigated via a combination of FTIR and Principal Component Analysis (PCA), and the results were compared with those obtained for the parent materials [**1**H]Cl and [**1**H]Br. All systems follow the same *nearly* first-order law, and the overall reaction kinetics is influenced by a subtle interplay of structural and electronic factors as well as other processes regulating the formation and lifetime of the reacting excimer.

Introduction

[2+2] photoreactions in crystalline materials are paradigmatic in solid-state photochemistry[1,2] and crystal engineering studies.[3,4] Since the pioneering work of Schmidt and Cohen,[5] who formulated the well-known topochemical postulate, i.e., maximum bond separation of 4.2 Å is a necessary condition for [2+2] cycloaddition to occur, these reactions have constantly attracted the curiosity of scientists, and have been at the core of intense debate concerning the mechanistic[6,7,8] and geometrical factors[9] affecting these kinds of transformations.

Over the last decades the focus has been mainly on the search of templating units able to pre-organize molecular double-bonds in the solid state, via non-covalent interactions such as hydrogen[10,11,12,13] and halogen bonds,[14,15,16] metal-coordination,[17,18,19,20] and also B-N bonds.[21] More recently, [2+2] cycloaddition reactions have been studied for applications such as conversion of light energy into mechanical work,[22] and synthesis of polymeric materials from natural molecules[23] or recovered from waste.[24] Among the widespread interest for cycloaddition reactions, the study of the [2+2] photoreactions involving solid solutions has remained rather unexplored; to the best of these authors' knowledge the number of literature reports is scarce, and concerning mainly the possibility of obtaining specific regioproducts.[25,26,27]

According to Kitaigorodsky[28] crystalline solid solutions can be defined as nonstoichiometric multicomponent crystals in which at least two components combine homogeneously in a unique phase with random occupancy of the crystallographic sites. The potential of solid solutions[29,30] as a tool for modifying the physicochemical properties of materials has been recently pointed out in several studies, including modulation of the thermosalient effect,[31] enantioselectivity,[32,33] polymorphic transition,[34,35] melting point,[36,37] and plastic phase transition,[38] among others.

We have recently reported on the activation of the solid-state photoreactivity in 4-aminocinnamic acid (**1**) through formation of molecular salts of general formula [**1**H]A, obtained by reacting **1** with a series of inorganic acids.[39,40,41] Interestingly, we have found that in the salts [**1**H]Cl and [**1**H]Br, obtained by reaction of **1** with the respective hydrohalic acid, [2+2] photoreactions are quantitative and occur in a single-crystal-to-single-crystal (SCSC) fashion, albeit at different rates (8 h for [**1**H]Cl *vs*. 4 h for [**1**H]Br).[39,40]

Intrigued by this feature, and taking advantage of the interchangeability in the solid state between the chloride and bromide anions, we explored the preparation of binary solid solutions with general formula [**1**H] Br_xCl_{1-x} ($0 < x < 1$), to investigate the effect of composition on the kinetics of the [2+2] photoreaction with respect to the parent materials. The crystalline solid-solutions have been prepared via mechanochemical methods and investigated by a combination of solid-state techniques, including single crystal and powder X-ray diffraction, micro-Raman, and FTIR-ATR spectroscopy. The combined use of these methods has made possible the correlation between the kinetics of the [2+2] SCSC photoreaction and the composition of the solid solutions.

Experimental

Synthesis. All reactants and reagents were purchased from Sigma-Aldrich, and used without further purification except 4-amino cinnamic acid (**1**) which was recrystallized from ethanol prior use. Reagent grade solvents and bi-distilled water were used.

[**1**H]Cl and [**1**H]Br: according to previously reported procedures[39,40] 200 mg (1.23 mmol) of 4-aminocinnamic acid (**1**) were suspended in ca. 5 mL of water and neutralized with the respective HX acid, undissolved material was filtered off, and the resulting solutions were left to slowly evaporate in the dark.
[**1**H]Br_xCl_{1-x} (binary solid solutions): the reactants were weighed in the proper stoichiometric ratio (see **Table 1**) and manually ground in presence of a catalytic amount of ethanol (kneading). Subsequently, the so-obtained crystalline materials were suspended in ca. 5 mL of water, sonicated up to complete dissolution and left to slowly evaporate in the dark. Single crystal suitable for XRD were obtained upon complete evaporation.

Table 1. Amounts of reagents used in the synthesis of binary solid solutions.

	[**1**H]Br	[**1**H]Cl
[**1**H]$Br_{0.25}Cl_{0.75}$	20.8 mg (0.09 mmol)	48.6 mg (0.24 mmol)
[**1**H]$Br_{0.5}Cl_{0.5}$	51.6 mg (0.21 mmol)	41.2 mg (0.21 mmol)
[**1**H]$Br_{0.75}Cl_{0.25}$	61.0 mg (0.25 mmol)	17.7 mg (0.09 mmol)

Single crystal X-ray Diffraction. Single-crystal data for [**1**H]Br_xCl_{1-x},before and after UV irradiation (see below), were collected at RT on an Oxford XCalibur S CCD diffractometer equipped with a graphite monochromator (Mo-Kα radiation, λ = 0.71073 Å). The structures were solved by intrinsic phasing with SHELXT[42] and refined on F^2 by full-matrix least squares refinement with SHELXL[43] implemented in Olex2 software.[44] H_{OH} and H_{NH} atoms were either directly located or, when not possible, added in calculated positions, H_{CH} atoms for all compounds were added in calculated positions and refined riding on their respective carbon atoms. In the crystal structure of the binary solid solutions the site occupancy factors (SOFs) of the anions were fixed according to those of the water solutions from which the mixed crystals were grown. Crystal structures of partially reacted crystal were treated as follows: (i) upon irradiation, new electron density peaks, consistent with the emergence of the photoproduct, appeared in the Delta Fourier Maps. The atoms of the disappearing reactant and appearing photoproduct were treated as disordered over two positions and refined anisotropically, refinement of the SOFs by adding a second free variable in the FVAR command line allowed the extraction of the dimer and reactant contents.

Data collection and refinement details are listed in **Errore. L'origine riferimento non è stata trovata.**. The program Mercury[45] was used to calculate intermolecular interactions and for molecular graphics. Crystal data can be obtained free of charge via www.ccdc.cam.ac.uk/conts/retrieving.html (or from the Cambridge Crystallographic Data Centre, 12 Union Road, Cambridge CB21EZ, UK; fax: (+44)1223-336-033; or e-mail: deposit@ccdc.cam.ac.uk). CCDC numbers 2038954-2038962.

Powder X-ray Diffraction. For phase identification purposes powder X-ray diffractograms in the 2θ range 5-30° (step size, 0.02°; time/step, 20 s; 0.04 rad soller; 40 mA x 40 kV) were collected on a Panalytical X'Pert PRO automated diffractometer equipped with an X'Celerator detector and in Bragg-Brentano geometry, using Cu Kα radiation without a monochromator. The program Mercury[45] was used for simulation of X-ray powder patterns on the basis of single crystal data determined in this work or retrieved from the CCDC database: PACPOB and for [**1**H]Cl and KEHFAH02 for [**1**H]Br. In all cases, the identity between polycrystalline samples and single crystals was always verified by comparing experimental and simulated powder diffraction patterns (see **Errore. L'origine riferimento non è stata trovata.**).

Solid State UV-irradiation. Single crystals samples were irradiated using a UV-LED (*Led EnginLZ1-10UV00-0000)* with λ = 365 nm and placed at a distance of 1 cm. The same light source and distance were used to irradiate powders for FTIR-ATR and single crystals for micro-Raman measurements. Powders were obtained by finely grinding in a mortar the crystalline material from the syntheses. A sufficient amount (about 1 mg) of powder was spread on a support and irradiated, taking care of frequently mixing it during the process to expose new surface and prevent the occurrence of surface phenomena only. Constant quantities of powder were analyzed by FTIR-ATR at intervals of 60 min until the spectrum either coincided with that of the pure dimer or did not show any further change.

FTIR-ATR spectroscopy. FTIR-ATR measurements in the wavenumber range 400-4000 cm^{-1} with a resolution of 0.5 cm^{-1} were carried out on a Perkin Elmer Spectrum Two spectrophotometer, equipped with a Universal ATR accessory. In Figure SI-3 the spectra of the [**1**H]Br monomer and of its dimer are compared, as a representative example of the spectra of the [**1**H]$Br_xCl_{(1-x)}$

series. In **Errore. L'origine riferimento non è stata trovata.** the bands corresponding to vibrational modes which disappear with the progress of the reaction are indicated.

Micro-Raman Spectroscopy. Raman spectra of the crystalline samples in the lattice phonon region (10-150 cm^{-1}) were collected with a Horiba Jobin Yvon T64000 triple monochromator spectrometer interfaced with the optical stage of an Olympus BX40 microscope. The excitation wavelength was a Kr^+ laser tuned at 647.1 nm set at very low power to avoid sample damage.

Principal Component Analysis (PCA) and the rate law. The PCA method employs an eigenvalue diagonalization procedure which, by analyzing the correlation of the data, decomposes the signal into a weighted sum of independent components (orthogonal to each other and therefore uncorrelated), ordered according to their contribution to the total variance. Important contributions are contained in the first few components. For our specific application to the analysis of the spectra[46] during the dimerization reaction, the first component mostly represents the contribution common to the spectra of both reactant and product and thus its weight remains nearly constant over time. The second component, which picks up the most important differences between the spectra, has a weight $w_{PCA}(t)$ which rapidly changes with time t and in fact describes the progress of the reaction. All further components collect the noise and can be ignored. A graphical representation of the PCA method is shown in **Errore. L'origine riferimento non è stata trovata.**5.

We have obtained the rate constants k reported in the results and discussion section by least square fitting $w_{PCA}(t)$ with a model $w_{FIT}(t)$ assuming a linear relationship with the unreacted fraction $\alpha(t)$ of the monomer, that is $w_{FIT}(t) = a\alpha(t) + b$, where, for the first order reaction which gave the best fit, $\alpha(t) = e^{-kt}$. The fitting parameters a, b and k where thus determined by minimizing $X^2 = \Sigma_t [w_{PCA}(t) - w_{FIT}(t)]^2 / \sigma_w^2$, with standard errors $\sigma_w \propto a$, i.e. constant standard errors σ_α on $\alpha(t)$.

The standard errors on the fitting parameter k reported in the result and discussion section have been estimated by jackknife "leave-one-out" resampling,[47] because the usual propagation of incertitudes (based on deviation from the fit, linearity, independence and normality assumptions)[48] is unreliable for highly non-linear procedures such as the PCA.

In addition to a first order law, the curves were tentatively fit also to an Avrami equation[49,50,51] in the form $\alpha(t) = e^{-kt^n}$, which coincides with the first order exponential decay when the additional parameter n takes the value 1. On releasing n, a smaller χ^2 is obtained as expected, but the lack of an improved quality of the fit can be judged by applying the Akaike Information Criterion AIC.[52] In fact, the choice of a model cannot be based solely on the agreement between measurement and fit; for instance, even though the experimental data could reproduced exactly by using a polynomial with number of terms (i.e. parameters) equal to the number of measurements, such a fit would contain no useful information beyond that already contained in the data. In some sense, we aim to maximize the additional information provided by the fit. A reasonable measure of the amount of information in a fit is the AIC (Akaike Information Criterion), defined as:

$$AIC = nln\chi^2 + 2K$$

where n is he number of experimental points (i.e. observations) and K is the number of adjustable parameters in the model. The model with the minimum AIC is regarded as the best representation of the experimental data. Thus, if different models yield similar χ^2 deviations, the smaller the number of parameters the lower the AIC. By choosing the model with the minimum AIC, one effectively combines a best fit criterion with a "principle of parsimony".

RESULTS And DISCUSSION

Crystalline [**1**H]Cl and [**1**H]Br are isomorphous,[39,40] therefore their crystal packings feature the same pattern of multiple charge-assisted hydrogen bonds (Figure ESI-1). In both crystals the [**1**H]$^+$ cations are properly aligned in an head-to-tail arrangement, with the double bonds at a distance of 3.657(5) Å and 3.618(6)Å for [**1**H]Cl and [**1**H]Br, respectively. Upon UV irradiation both crystals undergo an SCSC [2+2] photodimerization leading to the respective head-to-tail dimers [$\mathbf{1}_2H_2$]Cl_2 and [$\mathbf{1}_2H_2$]Br_2 (see Figure 1). The occurrence of the SCSC transformation in these systems can also be followed by analysis of the features displayed, upon irradiation, in the lattice phonon region (10-150 cm^{-1}) of the crystal vibrational spectrum, as determined also by the micro-Raman measurements (see Below).

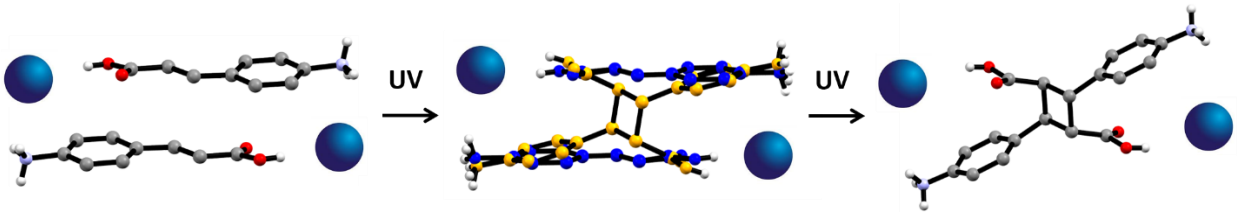

Figure 1. Representation of the [2+2] photodimerization occurring upon UV irradiation of single crystals of [**1**H]Cl and [**1**H]Br. H_{CH} omitted for clarity.

The differences in the reaction rate as a response to the different anion, and the isomorphism of [**1**H]Cl and [**1**H]Br prompted us to investigate (i) the possibility of obtaining solid solutions, via mechanochemistry and/or crystallization from solution, *over the entire range of composition*, and (ii)the effect of solid solution formation on the [2+2] photoreactivity.

Polycrystalline powders of [**1**H]Br and [**1**H]Cl were thus weighed in different stoichiometric ratios (see Table 1), subjected to mechanochemistry, recrystallized, and further analyzed with powder XRD to assess solid solution formation. Figure 2 shows a comparison between the XRD patterns of the parent materials and that of the 50:50 solid-solution, [**1**H]$Br_{0.5}Cl_{0.5}$, as an example. In this and in all the other cases the grinding process resulted in the physical mixture of the two starting phases, while kneading with a few drops of ethanol yielded solid solutions isomorphous with pure [**1**H]Cl and [**1**H]Br, as shown by powder diffraction patterns recorded on the solid products (see Figure 2).

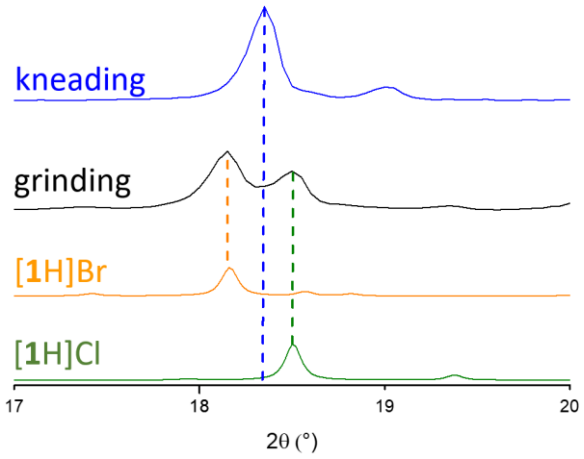

Figure 2. Detail of the experimental powder patterns for the [**1**H]$Br_{0.5}Cl_{0.5}$ solid solution obtained via kneading with ethanol, the physical mixture resulting from the grinding process, and the simulated patterns for the parent materials [**1**H]Br and [**1**H]Cl. The (002) peaks at 18.5° and 18.1° for [**1**H]Cl and [**1**H]Br, respectively, are still present in the physical mixture (black line), while they merge into one intermediate peak (blue line) upon formation of the [**1**H]$Br_{0.5}Cl_{0.5}$ solid solution.

Monitoring the position of the (002) reflection makes it possible to clearly appreciate how the patterns progressively shift to those of the pure components, thus reflecting a change in the unit cell volume as a function of the composition (Figures 3 and ESI-2). Additionally, solid solutions with 25:75, 50:50 and 75:25 stoichiometric ratios were obtained as single crystals from slow evaporation of aqueous solutions containing the two reactants [**1**H]Cl and [**1**H]Br. Based on a comparison of the unit cell constants (Table ESI-1), the two supramolecular salts are indeed miscible, leading to crystalline phases whose lattice parameters follow the Vegard's rule[53] in the whole composition range (Figure 3) and can be formulated as [**1**H]Br_xCl_{1-x} (with $0 < x < 1$).

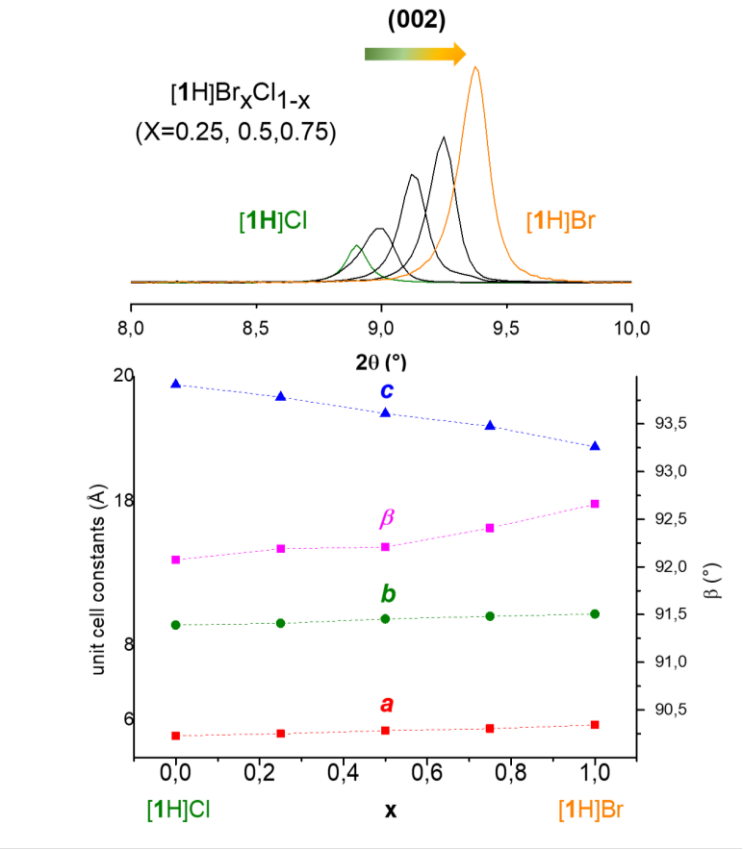

Figure 3. Top, detail of the PXRD patterns showing the shift of the (002) peak towards higher angles upon increasing the Br^- content. Bottom, relationship between the cell metrics and the Br^- content in [**1**H]Br_xCl_{1-x} (error bars are smaller than the markers).

For the crystalline solid solutions [**1**H]Br_xCl_{1-x} with x = 0.25, 0.5, and 0.75, we determined the structure via single-crystal XRD. The hydrogen bonding interaction patterns and the distances (d) between the double bonds present in the head-to-tail arrangements have remained approximately the same (Figure ESI-1) with respect to the starting materials [**1**H]Br and [**1**H]Cl.

The strong similarity among the structures of the series is also corroborated by the observed trend of their lattice phonon Raman spectra. Such data reflect structural changes by probing variations in lattice dynamics (Figure SI-4). Indeed, all the salts display nearly identical spectral features, and the cell volume contraction of [**1**H]Cl with respect to [**1**H]Br merely produces the blue shift of a couple of wavenumbers of the main peaks, which becomes hardly detectable in the solid-solutions. Therefore, the solid-solutions should still undergo [2+2] photoreactions.

To test their photoreactivity, the same single-crystals used for structure determination were irradiated simultaneously ex-situ for 2 h at 365 nm. Subsequent analysis on the irradiated specimens showed that the cyclization reaction had partially occurred via SCSC

in all cases, but unexpectedly with a different extent depending on the Br^-/Cl^- ratio. In these conditions, the reaction extent was estimated to be of ca 50% for [**1**H]$Br_{0.5}Cl_{0.5}$, while the remaining solid-solutions [**1**H]$Br_{0.25}Cl_{0.75}$ and [**1**H]$Br_{0.75}Cl_{0.25}$ showed ca 25% and 30%, respectively. Further irradiation resulted in the quantitative conversion and afforded the crystal structure of the corresponding photodimers [$\mathbf{1}_2H_2$]BrCl (ca 4 h more), [$\mathbf{1}_2H_2$]$Br_{1.5}Cl_{0.5}$ (ca 6 h more), [$\mathbf{1}_2H_2$]$Br_{0.5}Cl_{1.5}$ (overnight).

This prompted us to perform a detailed solid-state spectroscopic study to gain more insights into the kinetics of the pure parent salts and of the solid-solutions. We expected in this way to fully answer the second question, that is how solid solution composition impacts, in terms of time and mechanism, on the photoreactivity.

FTIR-ATR measurements were performed on the salt powders upon ex-situ irradiation. In Figure SI-3 we compare the spectra of [**1**H]Br and its photodimer [$\mathbf{1}_2H_2$]Br_2, obtained with an irradiation time long enough to assure a complete transformation of the reactant. The occurrence of the transformation is demonstrated by: (i) the shift of the stretching C=O band from 1693 cm^{-1} to 1699 cm^{-1} as a result of the loss of conjugation in the formation of the four member cycle; (ii) the disappearance of the vinyl C=C stretching band lying at about 1640 cm^{-1} and of the =C-H bending band at 1277 cm^{-1} [**1**H]Br.[54,55,56] Of course, the very crowded product and reactant spectra differ in a number of other features. As a typical example of the outcome of the kinetic study, Figure 4 shows a full set of spectra recorded as function of the irradiation time over the wavenumber range 1700-400 cm^{-1} for polycrystalline [**1**H]Br. Similar sequences have been collected for [**1**H]$Br_{0.75}Cl_{0.25}$, [**1**H]$Br_{0.5}Cl_{0.5}$, [**1**H]$Br_{0.25}Cl_{0.75}$ and [**1**H]Cl.

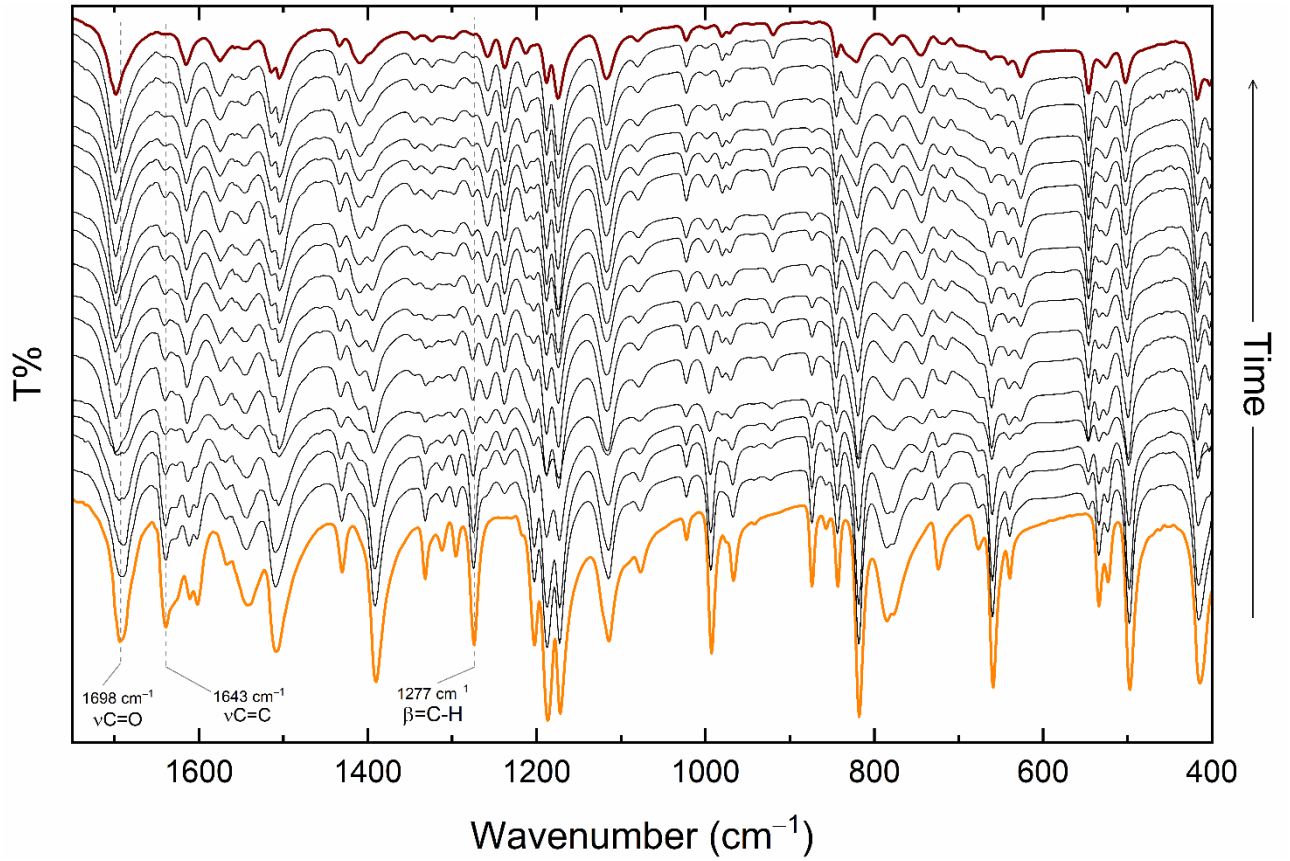

Figure 4. FTIR-ATR spectra of [**1**H]Br (orange-trace) as a function of the irradiation time (recorded at intervals of 60') in the wavenumber interval considered for the kinetics analysis (see text). The brown-trace identifies the pure dimer [$\mathbf{1}_2H_2$]Br_2. Vertical dashed lines indicate features mentioned in the text.

The most intuitive way to study the time progress of a chemical reaction from a series of spectra is to compare the spectra of the pure reactant and product, identify characteristic peaks of each species, and then use their intensity ratios as a function of time in the reactant/product mixtures to obtain concentration profiles that can be fitted to a kinetic law.[57] This method potentially discards the information contained in the overall differences among the spectra. For the FTIR data of this work, such a problem was solved by obtaining the unreacted monomer fraction $\alpha(t)$ as a function of the irradiation time t by means of the principal component analysis (PCA) approach,[46] as reported in detail in the ESI. Figure 5 reports the fractions $\alpha(t)$ *vs* t for the salts under investigation. All of them are well described by a first order kinetics $\alpha(t) = e^{-kt}$. The curves resulting from the fits are also shown in the Figure while the rate constants k are given in the inset of Figure 5. As reported in the ESI, the data do not justify kinetics different from a first order model.

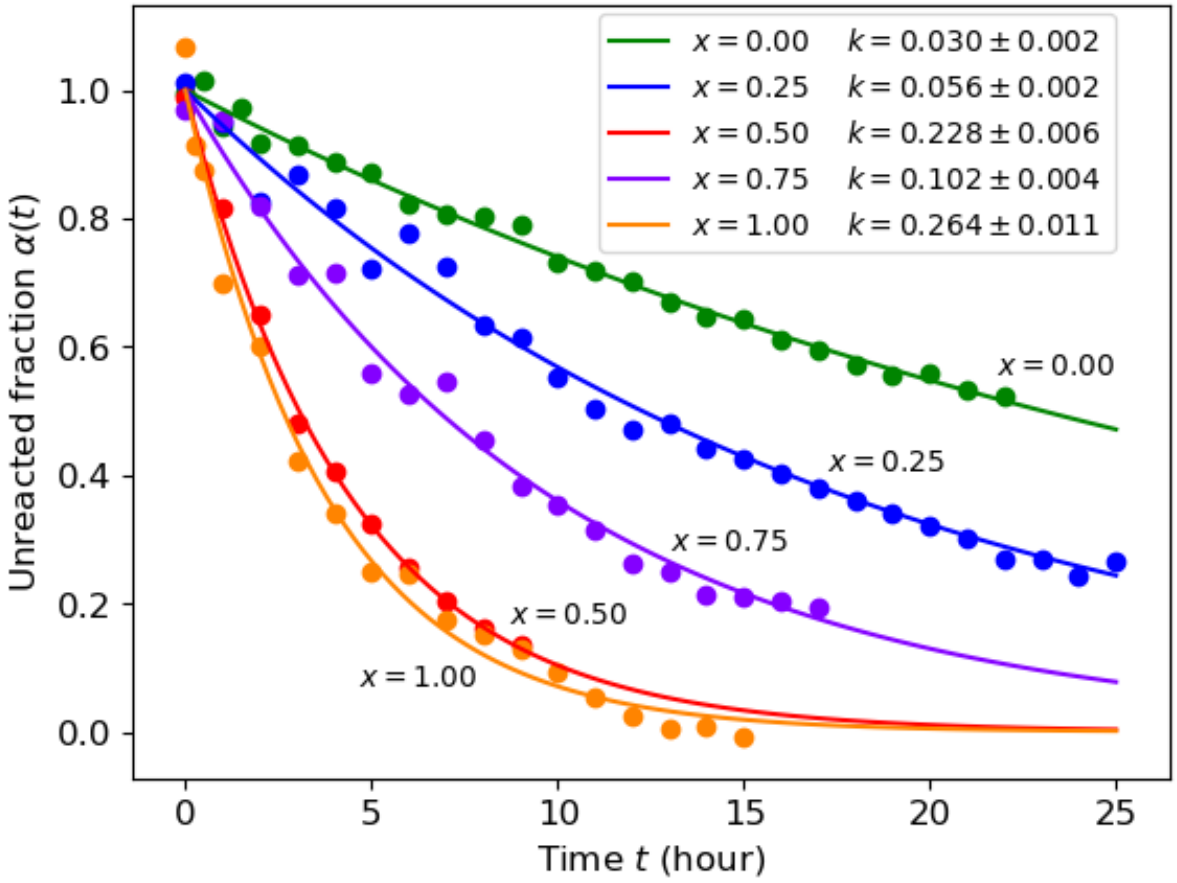

Figure 5. Unreacted fraction α(*t*) of the [**1**H]$Br_xCl_{(1-x)}$ monomers as a function of irradiation time *t*; dots: estimates from the PCA of the experimental spectra; curves: exponential decays from the fits with a first order kinetic law $\alpha(t) = e^{-kt}$. Inset, first order kinetic constants *k* (h^{-1}) as deduced by fitting the PCA results for the FTIR-ATR spectra of [**1**H]$Br_xCl_{(1-x)}$ in the wavenumber interval 400-1750 cm^{-1}, with standard deviations estimated by jackknife resampling.[47]

Thus, in all cases we can assume the monomer concentration to decay with a kinetics law close to a first order. To understand the origin of this, we can consider the overall reaction mechanism, as illustrated in Figure 6. The steps are: (1) upon light absorption, the monomer M transforms into the excited monomer M* (rate constant $k_1 I_v$, where I_v is the light beam intensity); (2) spontaneous de-excitation from M* back to M (rate k_2); (3) reversible reaction of M* and M molecules which combine to form the excimer (MM)*(rates k_3, k_4): note that such a process may involve the excitonic transport of the activation energy to sites far from that initially excited. Finally (4), the excimer can decay to form the dimer D (rate k_5).

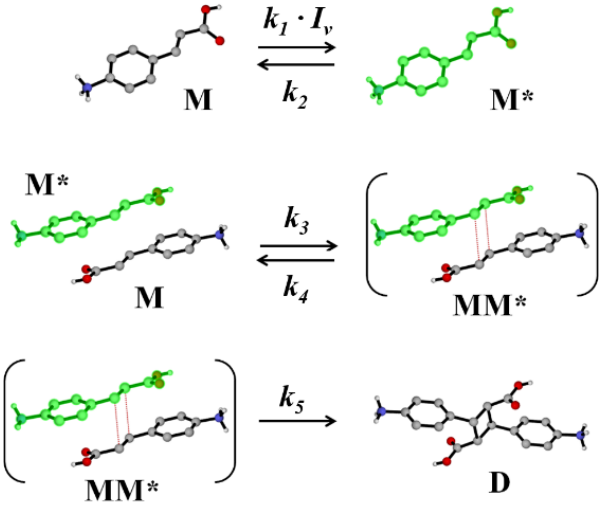

Figure 6. Representation of the overall [2+2] photodimerization occurring upon UV irradiation of crystalline samples of [**1**H] Br_xCl_{1-x}. H_{CH} omitted for clarity. I_v is the light beam intensity.

The full set of rate equations governing steps (1)-(4) are reported in ESI. Under steady state conditions for the excited species M* and MM*, the kinetic law yielding the decay of the monomer M is found to be:

$$\frac{d[M]}{dt} = \frac{-2k_1 I_v k_3 k_5 [M]^2}{k_2(k_4 + k_5) + k_3 k_5 [M]} = -2k_1 I_v \frac{[M]^2}{K + [M]} \qquad (1)$$

where $K = \frac{k_2(k_4+k_5)}{k_3 k_5}$

The reaction appears of pseudo second order in $[M]$ for $[M] \ll K$. Instead for $[M] \gg K$ a pseudo first order is obtained, and this corresponds to a very small k_2 and/or a large k_3. Clearly the introduction of a spontaneous decay of the excited monomer (i.e. k_2>0) is needed to have a non-trivial kinetics, that could be described as a process in which the absorption of every photon produces and exciton reacting with a molecule M. The experimental differences detected in the reactivity of the various salts must result from the different rates of the single steps, which contribute to the effective rate constants, even though the result of a photoinduced transformation, especially one in the solid state, can only be understood as the interplay of several processes.

The lower reactivity of [**1**H]Cl might be rationalized in terms of packing "compactness", which is linked to the reaction cavity size, as well as number and strength of the hydrogen-bonds between the -NH_3^+ and -COOH groups, located on the reactive molecules, and the halides. In this sense, a strong hydrogen-bond acceptor, such as the Cl^-,[58,59] could offer more resistance to the molecular rearrangements occurring during the photocyclization, thus making the reaction hindered. On the other hand, an anion such as Br^-, which is a weaker hydrogen-bond acceptor,[5859] should favor molecular migration while maintaining the hydrogen bonding interactions during the monomer to dimer transformation, thus speeding up the all process. Similarly, a more “compact” packing should reduce the reaction cavity volume and could, in principle, offer more resistance to such rearrangements, making the reaction disfavored again.[23]

Indeed, with a probe radius of the algorithm implemented in Mercury[45] set to 0.6, a void occupying 0.8% of the unit cell volume can be found in [**1**H]Br, while in the solid-solutions the same quantity ranges between 0.7 and 1.4%. With the same settings, the [**1**H]Cl structure displays a smaller void, accounting for the 0.4% of the unit cell volume, which makes this phase the most efficiently packed in the series, and consequently also with a smaller reaction cavity. The lower reactivity of chloride salt also reflects in the lower reactivity of the solid-solutions, for none of them shows kinetics as fast as [**1**H]Br's. Noteworthy, the trend is not monotonic, as [**1**H]$Br_{0.5}Cl_{0.5}$ has, unexpectedly, the highest kinetic constant among the series. Because of the 1:1 ratio between the chloride and bromide anions, such a phase might be regarded as a "pseudo" stoichiometric multicomponent crystal, hence possessing slightly different features compared to the other solid-solutions. However, the halide positions result to be indistinguishable by XRD, even by lowering the symmetry down to the triclinic system (P1) and refining the halides SOFs. This leaves this phase peculiar behavior not fully explained.

FTIR ATR spectroscopy, holding the advantage of analysis easiness and speed, is a useful technique for identifying the species in the course of the chemical reaction but provides no information about the lattice transformation that takes place with it. On the other hand, micro-Raman spectroscopy in the lattice phonon range may provide information about the related lattice transformation.[57,60,61,62]

As an example, Figure 7 shows the evolution of the [**1**H]Br lattice phonon Raman spectrum under irradiation. The band at 21 cm^{-1} loses intensity and gradually shifts up to 26 cm^{-1}, while that at 38 cm^{-1} disappears and those at higher wavenumbers (in the range 75-100 cm^{-1}) merge together into a broad envelope. The spectrum of lattice vibrations changes continuously, evolving from that of the reagent to that of the product and therefore the spectra sequence cannot be solved as the sum of spectra of the two. This behavior is at variance from what observed in solid state reactions that take place with a phase reconstruction mechanism,[57,60,61,62] where the lattice phonons of both reactant and product appear in the spectrum as long as the host (the reactant) and the guest (the product) phases coexist. Thus, this evidence agrees with a picture in which at each moment of the SCSC transformation the system consists of a solid solution of monomer and dimer.

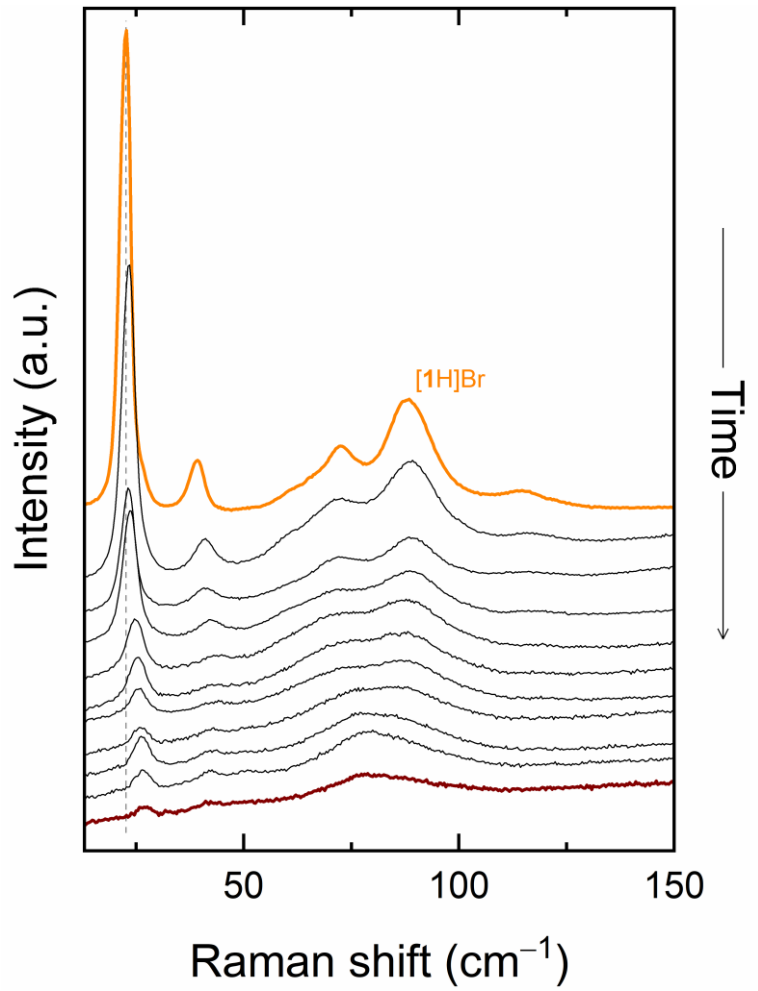

Figure 7. Raman spectra in the lattice phonon interval of a single crystal of [**1**H]Br under irradiation. The spectra have been recorded at time intervals of 10'. The orange trace identifies the pure monomer [**1**H]Br; the brown trace the pure dimer [$\mathbf{1}_2H_2$]Br_2. The vertical line marks the shift of the lattice phonon band at 20 cm^{-1} in the monomer with the advancement of the reaction.

Conclusions

In this paper we have reported our findings on the solid-state [2+2] photoreactivity of the 4-aminocinnamic acid solid-solutions with general formula [**1**H]Br_xCl_{1-x} ($0 < x < 1$). These salts were obtained as crystalline materials through mechanochemistry by mixing the parent compounds, [**1**H]Br and [**1**H]Cl in different molar ratios. The unit cell constants showed a linear response with composition; this behavior is typical of solid-solutions and of crystals constructed by almost isostructural species. For all the solid-solutions, single crystals were also proved to undergo an SCSC photoreaction upon UV exposure.

To investigate the effect of the solid-solutions composition on the kinetics of the [2+2] photoreaction, FTIR-ATR data collected upon irradiation were treated using the PCA method. Monomer and dimer vibrational spectra are very crowded and similar, so that the maximum information on the reaction progress is obtained from the entirety of the spectral features, rather than a limited number of bands assumed as diagnostic. The analysis has allowed us to derive a kinetic law in agreement with a very plausible reaction scheme and to quantify the rate differences displayed by the salts. All systems obey to the same kinetics, which is satisfactorily described as a nearly first order. However, in treating solid state reactions, one should consider that the true system is often too

complex and is not adequately described in terms of elementary steps. Structural features and material properties justify the varying reactivity along the series. [**1**H]Cl very low reactivity links with the highest packing "compactness", and the maximum number of the stronger hydrogen-bonding interactions, namely those between the between the $-NH_3^+$ and -COOH groups, located on the monomers, and the chloride. The photoreactive behavior of [**1**H]$Br_{0.5}Cl_{0.5}$, which has proved to be the fastest compared to the other two solid-solutions, namely [**1**H]$Br_{0.25}Cl_{0.75}$ and [**1**H]$Br_{0.75}Cl_{0.25}$, represents an exception.

In conclusion, such results suggest that the overall reaction kinetics is in fact governed by a subtle interplay involving structural and electronic factors such as the small voids left within the structure, the type and strength of the charge assisted hydrogen bonding interactions as well as other processes which regulate the formation and the lifetime of the reacting excited state, i.e. the excimer. From these authors' knowledge, this research represents the first attempt to tuning the speed of the [2+2] photoreactivity by using solid-solutions expanding, thus, the study of such reactions in non-stoichiometric crystalline materials. Work is in progress to extend such an approach to other solid-solutions made-up of components prone to undergo photocyclization, including those systems which proceed via a non-topochemical mechanism.

Conflicts of interest

There are no conflicts to declare.

Acknowledgements

We acknowledge financial support from the University of Bologna.

Notes and References

1 M. D. Cohen, *Tetrahedron*, 1987, **43**, 1211–1224.

2 J. M. Cole and M. Irie, *CrystEngComm*, 2016, **18**, 7175–7179.

3 D. Braga, F. Grepioni, L. Maini and S. d'Agostino, *Eur. J. Inorg. Chem.*, 2018, **2018**, 3597–3605.

4 G. R. Desiraju, *J. Am. Chem. Soc.*, 2013, **135**, 9952–9967.

5 M. D. Cohen, G. M. J. Schmidt and F. I. Sonntag, *J. Chem. Soc.*, 1964, 1996–2000.

6 G. Kaupp, *Int. J. Photoenergy* 2001, **3,** 55-62.

7 M. K. Mishra, A. Mukherjee, U. Ramamurty and G. R. Desiraju, *IUCrJ* **2**, 2015, 653–660.

8 D. De Loera, A. Stopin and M. A. Garcia-Garibay, *J. Am. Chem. Soc.*, 2013, **135**, 6626–6632.

9 S. Y. Yang, P. Naumov and S. Fukuzumi, *J. Am. Chem. Soc.*, 2009, **131**, 7247–7249.

10 G. Campillo-Alvarado, C. Li, D. C. Swenson and L. R. Macgillivray, *Cryst. Growth Des.*, 2019, **19**, 2511–2518.

11 D. Braga, S. DAgostino and F. Grepioni, *Cryst. Growth Des.*, 2012, **12**, 4880–4889.

12 L. R. Macgillivray, G. S. Papaefstathiou, T. Friščić, T. D. Hamilton, D. K. Bučar, Q. Chu, D. B. Varshney and I. G. Georgiev, *Acc. Chem. Res.*, 2008, **41**, 280–291.

13 T. Friščić, E. Elacqua, S. Dutta, S. M. Oburn and L. R. MacGillivray, *Cryst. Growth Des.*, 2020, **20**, 2584–2589.

14 T. Caronna, R. Liantonio, T. A. Logothetis, P. Metrangolo, T. Pilati and G. Resnati, *J. Am. Chem. Soc.*, 2004, **126**, 4500–4501.

15 J. Quentin and L. R. MacGillivray, *ChemPhysChem*, 2020, **21**, 154–163.

16 J. Quentin and L. R. MacGillivray, *Cryst. Growth Des.*, 2020, **20**, 7501−7515.

17 I. H. Park, K. Sasaki, H. S. Quah, E. Lee, M. Ohba, S. S. Lee and J. J. Vittal, *Cryst. Growth Des.*, 2019, **19**, 1996–2000.

18 K. Yadava and J. J. Vittal, *Chem. - A Eur. J.*, 2019, **25**, 10394–10399.

19 I. G. Georgiev, D. K. Buar and L. R. MacGillivray, *Chem. Commun.*, 2010, **46**, 4956–4958.

20 C. Li, G. Campillo-Alvarado, D. C. Swenson and L. R. Macgillivray, *Inorg. Chem.*, 2019, **58**, 12497–12500.

21 G. Campillo-Alvarado, C. Li, Z. Feng, K. M. Hutchins, D. C. Swenson, H. Höpfl, H. Morales-Rojas and L. R. Macgillivray, *Organometallics*, 2020, **39**, 2197–2201.

22 K. Yadava and J. J. Vittal, *Cryst. Growth Des.*, 2019, **19**, 2542–2547.

23 V. Ramamurthy and J. Sivaguru, *Chem. Rev.*, 2016, **116**, 9914–9993.

24 K. Randazzo, Z. Wang, Z. D. Wang, J. Butz and Q. R. Chu, *ACS Sustain. Chem. Eng.*, 2016, **4**, 5053–5059.

25 T. B. Nguyen and A. Al-Mourabit, *Photochem. Photobiol. Sci.*, 2016, **15**, 1115–1119.

26 D. K. Bucar, A. Sen, S. V. S. Mariappan and L. R. Mac Gillivray, *Chem. Commun.*, 2012, **48**, 1790–1792.

27 C. R. Theocharis, G. R. Desiraju and W. Jones, *J. Am. Chem. Soc.*, 1984, **106**, 3606–3609.

28 A. I. Kitaigorodsky, ed. J. Ebenezar, Springer, Berlin, Heidelberg, Cham, 1984, pp. 563–598.

29 M. Lusi, *Cryst. Growth Des.*, 2018, **18**, 3704–3712.

30 M. Lusi, *CrystEngComm*, 2018, **20**, 7042–7052.

31 E. Nauha, P. Naumov and M. Lusi, *CrystEngComm*, 2016, **18**, 4699–4703.

32 T. Rekis, S. D'Agostino, D. Braga and F. Grepioni, *Cryst. Growth Des.*, 2017, **17**, 6477–6485.

33 T. Rekis, A. Berziņš, I. Sarceviča, A. Kons, M. Balodis, L. Orola, H. Lorenz and A. Actiņš, *Cryst. Growth Des.*, 2018, **18**, 264–273.

34 A. Delori, P. Maclure, R. M. Bhardwaj, A. Johnston, A. J. Florence, O. B. Sutcliffe and I. D. H. Oswald, *CrystEngComm*, 2014,

16, 5827–5831.

35 S. d'Agostino, L. Fornasari, F. Grepioni, D. Braga, F. Rossi, M. R. Chierotti and R. Gobetto, *Chem. - A Eur. J.*, 2018, **24**, 15059–15066.

36 A. K. S. Romasanta, D. Braga, M. T. Duarte and F. Grepioni, *CrystEngComm*, 2017, **19**, 653–660.

37 E. Schur, E. Nauha, M. Lusi and J. Bernstein, *Chem. - A Eur. J.*, 2015, **21**, 1735–1742.

38 S. D'Agostino, L. Fornasari and D. Braga, *Cryst. Growth Des.*, 2019, **19**, 6266–6273.

39 S. D'Agostino, F. Spinelli, E. Boanini, D. Braga and F. Grepioni, *Chem. Commun.*, 2016, **52**, 1899-1902.

40 S. D'Agostino, P. Taddei, E. Boanini, D. Braga and F. Grepioni, *Cryst. Growth Des.*, 2017, **17**, 4491–4495.

41 S. D'Agostino, E. Boanini, D. Braga and F. Grepioni, *Cryst. Growth Des.*, 2018, **18**, 2510–2517.

42 G. M. Sheldrick, *Acta Crystallogr. Sect. A Found. Crystallogr.*, 2015, **71**, 3–8.

43 G. M. Sheldrick, *Acta Crystallogr. Sect. C Struct. Chem.*, 2015, **71**, 3–8.

44 O. V. Dolomanov, L. J. Bourhis, R. J. Gildea, J. A. K. Howard and H. Puschmann, *J. Appl. Crystallogr.*, 2009, **42**, 339–341.

45 C. F. Macrae, I. J. Bruno, J. A. Chisholm, P. R. Edgington, P. McCabe, E. Pidcock, L. Rodriguez-Monge, R. Taylor, J. Van De Streek and P. A. Wood, *J. Appl. Crystallogr.*, 2008, **41**, 466–470.

46 K. H. Kim, J. G. Kim, S. Nozawa, T. Sato, K. Y. Oang, T. W. Kim, H. Ki, J. Jo, S. Park, C. Song, T. Sato, K. Ogawa, T. Togashi, K. Tono, M. Yabashi, T. Ishikawa, J. Kim, R. Ryoo, J. Kim, H. Ihee and S. I. Adachi, *Nature*, 2015, **518**, 385–389.

47 H. Babamoradi, F. Van Den Berg and Å. Rinnan, *Chemom. Intell. Lab. Syst.*, 2013, **120**, 97–105.

48 W. H. Press, S. a. Teukolsky, W. T. Vetterling and B. P. Flannery, *Numerical Recipes in Fortran 77: the Art of Scientific Computing. Second Edition*, 1996, vol. 1.

49 M. Avrami, *J. Chem. Phys.*, 1939, **7**, 1103–1112.

50 M. Avrami, *J. Chem. Phys.*, 1940, **8**, 212–224.

51 M. Avrami, *J. Chem. Phys.*, 1941, **9**, 177–184.

52 K. P. Burnham and D. R. Anderson, *Sociol. Methods Res.*, 2004, **33**, 261–304.

53 A. R. Denton and N. W. Ashcroft, *Phys. Rev. A*, 1991, **43**, 3161–3164.

54 Z. Wang, K. Randazzo, X. Hou, J. Struppe, A. Ugrinov, B. Kastern, E. Wysocki and Q. R. Chu, 2015.

55 K. Randazzo, Z. Wang, Z. D. Wang, J. Butz and Q. R. Chu, *ACS Sustain. Chem. Eng.*, 2016, **4**, 5053–5059.

56 L. Devi, V. Arjunan, M. K. Marchewka and S. Mohan, in *Springer Proceedings in Physics*, ed. J. Ebenezar, Springer International Publishing, Cham, 2017, vol. 189, pp. 563–598.

57 T. Salzillo, S. Zaccheroni, R. G. Della Valle, E. Venuti and A. Brillante, *J. Phys. Chem. C*, 2014, **118**, 9628–9635.

58 A. Allerhand and P. von R. Schleyer, *J. Am. Chem. Soc.*, 1963, **85**, 1233–1237.

59 G. A. Jeffrey, W. Saenger, G. A. Jeffrey and W. Saenger, in *Hydrogen Bonding in Biological Structures*, eds. G. A. Jeffrey and W. Saenger, Springer Berlin Heidelberg, Berlin, Heidelberg, 1994, pp. 161–163.

60 T. Salzillo and A. Brillante, *CrystEngComm*, 2019, **21**, 3127–3136.

61 T. Salzillo, I. Bilotti, R. G. Della Valle, E. Venuti and A. Brillante, *J. Am. Chem. Soc.*, 2012, **134**, 17671–17679.

62 T. Salzillo, E. Venuti, R. G. Della Valle and A. Brillante, *J. Raman Spectrosc.*, 2017, **48**, 271–277.